OPEN ACCESS
International
Journal
Of Modern Engineering Research (IJMER)

Numerical simulation on aerodynamic drag of high-speed trains in single track tunnel

Junguo Wang*, Yuchen Bai
School of Mechanical Engineering, Southwest Jiaotong University, Chengdu 610031

***Abstract**: Taking a certain type of high-speed electric train (HSET) of China as the research object, based on the basic theory of aerodynamics, a three-dimensional unsteady compressible flow N-S equation and a Realizable k-ε turbulence model are adopted to establish an aerodynamic simulation model for theHSET3-car formation with different speed of 200 km/h and 300 km/h. The transient velocity field and aerodynamic drag characteristics of a single HSET in single track tunnel are studied by using fluid dynamics analysis software for aerodynamic simulation. It is found that a significant train wind would form around the train, with an increase in wind thickness and vortex separation along the direction from the head car (HC) to the tail car (TC). When the HSET runs the tunnel and the expansion wave generated by the TC entering the tunnel reaches the HC, the maximum drag of the HSET reaches 44.52kN.*

***Keywords:** High-speed electric train (HSET), turbulence model, velocity field, vortex.*

Date of Submission: 19-12-2024 Date of acceptance: 24-02-2025

I. Introduction

With the continuous increase of train speed, the aerodynamic problems of trains are gradually becoming more prominent. Due to the viscous effect of air, when a train runs in tunnel, the air in the boundary layer move together with the train, and the train wind formed may harm tunnel equipment and personnel, meanwhile the train may experience skidding or bumps due to aerodynamic forces, which may pose a threat to the stability and safety of the HSET operation. How to reduce the aerodynamic drag of HSET is the key to improving their operational efficiency and reducing energy consumption.

Aerodynamic characteristics of HSET can be obtained by moving train or simulation model tests. Muldet al. (2012) studied the wake characteristics of trains using the separated vortices method based on the STAR-CCM+software. Chu et al. (2014) adopted a three-dimensional compressible turbulence model and the sliding mesh method to achieve the relative motion between the train and the tunnel, and analyzed the aerodynamic characteristics during train intersection. Kikuchiand Suzuki (2015) designed wind tunnel tests under different operating conditions to study the aerodynamic forces of high-speed trains, including windshields, pantographs, and bodies. Soper et al. (2015) studied the external flow characteristics of high-speed trains in a wind tunnel using a scaled model. Bell et al. (2015) conducted a scaled dynamic model experiment to study the train wake of high-speed trains, revealing differences between the results of the scaled dynamic model and the full-scale model.

HSET aerodynamics is the basic science for solving the bottleneck problem of development of high-speed railway. Li et al. (2024) used segregated incompressible large-eddy simulation and acoustic perturbation equations to obtain the flow field and sound field of 1:25 scale trains in a long tunnel, also the aerodynamic simulation results were verified by wind tunnel test. Xie et al. (2020) conducted dynamical model tests to collect the interior pressure transients under different speeds of HSET. Ferrari et al. (2017) presented a novel surface visualization to convey the spatiotemporal changes undergone by clustered vortices in the wake of high-speed trains. Wu et al. (2022) investigated the transient aerodynamic characteristics of a high-speed train moving in a truss girder bridge and passing by a bridge tower in a wind tunnel, which the scaled ratio of the train, bridge, and tower were 1:30. Niu et al. (2021) compared and analyzed the aerodynamic forces on a stationary train and moving train as well as the flow fields at the bottom of the trains.

In the past, research mainly focused on the pressure flow field around the upper or lower part of the train, the aerodynamic drag of high-speed trains in single track tunnel is not much considered. In this study, a

three-dimensional unsteady compressible flow N-S equation and a Realizable k-ε turbulence model are adopted to establish an aerodynamic simulation model for the HST 3-car formation with a speed of 300 km/h. To provide simulation results for aerodynamic design, the transient velocity field and aerodynamic drag characteristics of a single train are also compared and analyzed.

II. Turbulence model of the HSET

The flow phenomenon related to high-speed trains (HSET) is turbulent flow with high Reynolds number, which is a dimensionless coefficient that characterizes the viscous flow characteristics around the train. When the minimum speed of the train is selected as 300 km/h, the width of the train is 3.4 m, and the viscosity coefficient of air motion is 15.08×106 m2/s, it can be calculated that the Reynolds number of the external flow field of the HSET is about 1.879×106. Therefore, the outflow field of HSET is in a turbulent state, and the calculation model must use a turbulent model.

Turbulence model simulation are generally divided into direct numerical simulation (DNS) and non-direct numerical simulation. The DNS has very high requirements for memory space and computing speed, which makes it difficult to use for true engineering calculations at present. The NDNS mainly includes Reynolds averaged numerical simulation (RANS), large eddy numerical simulation (LES) and detached eddy simulation (DES).The RANS describe turbulence model through time averaged Navier-Stokes equations to avoid the problem of high computational complexity in DNS methods, and the LES simulates large-scale eddy in turbulence directly using the instantaneous N-S equation, while the influence of small eddy on large eddy is considered through an approximate model. The DES combines the advantages of LES and RANS, in which the RANS and the LES is separately used in the near wall region and in the mainstream region far from the wall. The DES has advantages including the resolution of log-layer mismatches and grid-induced separation, and is therefore widely adopted to simulate the aerodynamic characteristics of high-speed trains. The flow field around the high-speed train is turbulent flow, the DES based on the Realizable k–ε turbulence model is used to simulate the unsteady aerodynamic performance of the HSET in this study. They are calculated using the following formulas

$$\begin{aligned} &\mathrm{Re}=\rho v_m L/\mu, \quad I=0.16\,\mathrm{Re}^{-0.125}, \\ &k=1.5\times(Iv_{\mathrm{m}})^2, \quad \varepsilon=C_0^{3/4}k^{3/2}L \end{aligned} \tag{1}$$

where Re is the Reynolds number, ρ is air density with ρ=1.225kg/m3 at 15°C, v_{m} is the average incoming velocity, L is the train scale and is equal to H, μ is the air viscosity coefficient with μ=1.8×10-5kg/m3, *I* is the turbulence intensity, C0 represents the empirical constant and is equal to 0.09.

III. Computational model and boundary conditions

3.1 Computational model

HSTs are usually composed of 8 or 16 cars, but when conducting numerical simulations, longer trains can significantly increase computation time and costs. Due to the unchanged cross-section of the middle car in HSET, the shortened train model will not alter the structural characteristics of the flow field. To study the flow characteristics of the flow field around the bogie during HSET operation and its contribution to the total aerodynamic drag value of the train, irregular components such as pantographs and handrails on the train surface are removed during geometric modeling, while structures such as windshields and bogies are retained. The HSET model consists of t head car (HC), middle car (MC) and tail car (TC) as shown in Figure 1,where the height (H),length, and width of the train are 3.7m, 76.4m(20.7H) and 3.4m,respectively.

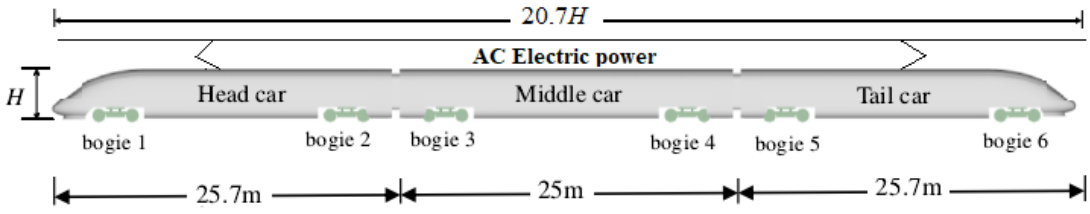

Figure 1. Model of the proposed high-speed train

Different types of body grids in computational fluid dynamics (CFD) software are calculated using Trim and Prism layer body grids based on trial calculations. The entire spatial computing domain adopts a larger mesh size, and mesh refinement is carried out in areas with large flow field changes, with a layer by layer

transition scheme from fine mesh to coarse mesh. For the near wall area of the train surface, the thickness of the first layer of the wall boundary layer can be calculated by the following formula,

$$\Delta y = \sqrt{80} L y^{+} \Big/ \mathrm{Re}_{L}^{13/14} \tag{2}$$

where y+ represents dimensionless parameter. Hence, a fifteen layers of boundary layer are set on the surface of the HSET body, which the distance from the first layer of grid near the wall to the wall is 0.5 mm, and the computational model adopts hexahedral unstructured mesh and prismatic layer mesh, as displayed in Figure 2.

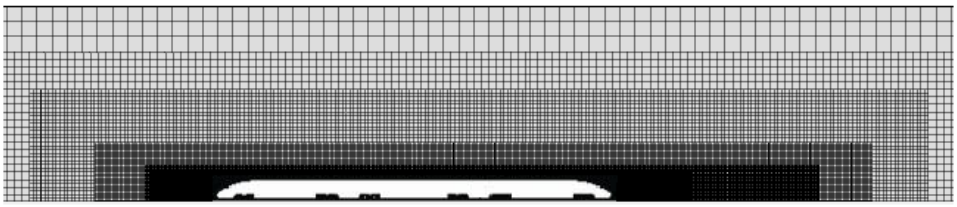

(a) Cross-sectional mesh of the calculation area

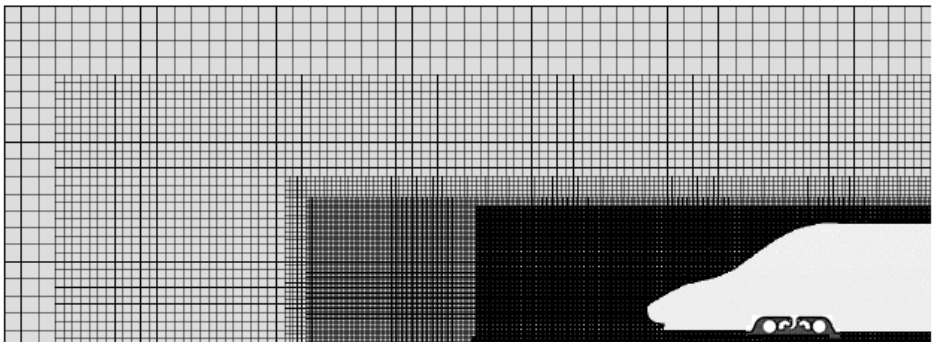

(b) Surface grid of the train body

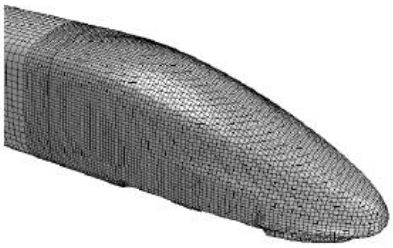

(c) Grid of train head

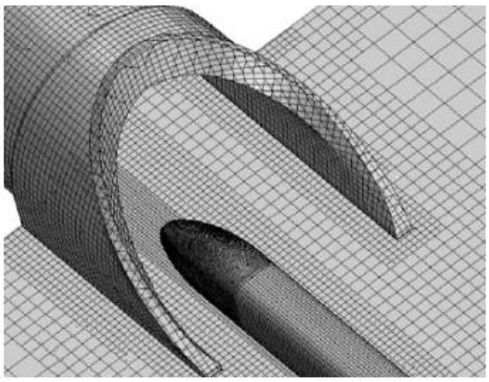

(d) Grid of tunnel entrance

Figure 2. Mesh generation and computational domain

3.2 Boundary conditions

To ensure the full development of the flow field and avoid the influence of boundaries on the flow field structure around the train, the length of the calculation domain in the X direction is set to 70H, the width in the Y direction is 20H, and the height in the Z direction is 20H. To avoid the influence of the entrance boundary, the nose tip of the train head is set to 18H away from the entrance boundary, the calculation domain of the HSET is shown in Figure 3(a).

The simulation area includes the HSET operating without and with tunnels. Considering the calculation accuracy and efficiency, the length, width, and height of non-tunnel area are set to 200 m, 80 m, and 40 m, respectively, as shown in Figure 3(b).The simulation of the external speed flow field of the HSET is analyzed from four typical positions, including the HSET runs in non-tunnel area (defined as P1), the HC enters the tunnel (P2), the HSET runs in tunnel area (P3), and the HC exits the tunnel (P4).

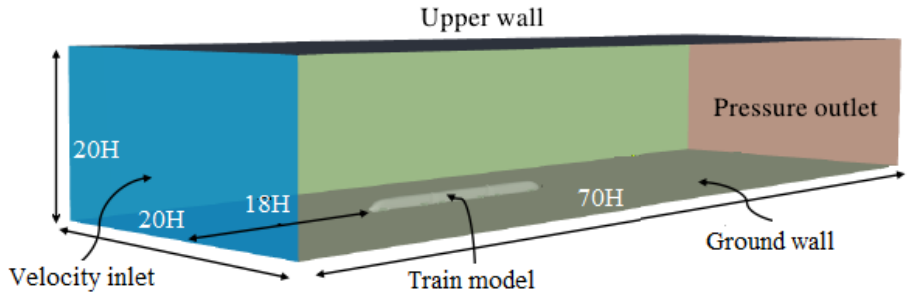

(a) Computational domain

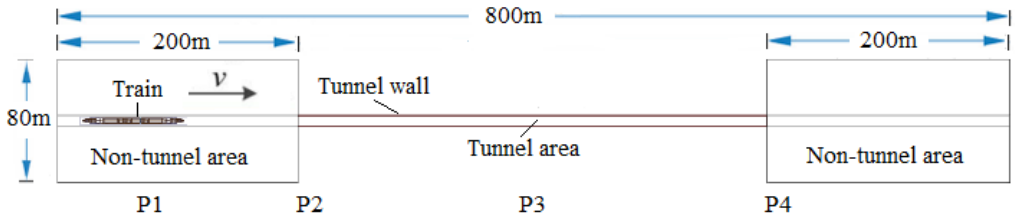

(b) Boundary conditions

Figure 3. Computational domain and boundary conditions

The boundary conditions that need to be determined include velocity inlet, pressure outlet, and wall boundary conditions. In this study, the surface of the train is set as a non-slip wall boundary condition, the top and both sides of the watershed are set as symmetrical boundaries, and the front end of the watershed is set as a velocity inlet boundary. The velocity is set as follows, the X-direction velocity component is the average incoming velocity v_m, and the Y-direction and Z-direction velocity components are both zero.

3.3 Aerodynamic coefficients

The proposed aerodynamic coefficients mainly include drag coefficient C_d, which is defined as following form

$$C_d = F_d / (0.5 \rho v_m S) \tag{3}$$

where F_d is the aerodynamic drag, S is the reference area of the train cross-section, and it is equal to 0.17375 m^2 for the 1:8 scaled HSET model.

IV. Calculation results and analysis

4.1 External speed field of the HSET

When the HC runs in non-tunnel areas, it can be observed from Figure 4that the fluid flow direction is centered around the curved body of the HC, forming a spherical wave that flows in all directions. Meantime, the fluid at the junction of the straight and curved body of the HC gradually flows towards the direction of the TC, and the fluid on both sides of the HSET begins to rotate in opposite directions at the junction of the straight and curved body of the HC.

When the HSET runs in non-tunnel areas, the thickness of the boundary layer of the HSET speed gradually increases along the length direction of the HSET as shown in Figure 5. At the same time, vortices appear in the fluid on both sides of the HSET, and the vortex range gradually increases as it moves away from the HC, which can be understood as the generation and dissipation of vortices. Obviously, when the HSET runs on the non-tunnel areas, it still conforms to the Karman vortex street.

When the HC enters the tunnel, the fluid at the tunnel entrance is compressed after the HC enters the tunnel entrance, and the fluid propagates in the form of spherical waves around the curved body of the HC as an approximate center as shown in Figure 6. When the fluid encounters the tunnel wall, a portion of the fluid flows forward in the direction of the tunnel exit, while another portion flows out in the direction of the tunnel entrance, the velocity of the fluid around the curved body of the HC also increases.

When the HSET runs inside the tunnel, it can be observed from Figure 7 that the boundary between the curved body and the windshield near the nose of the HC is located, and the fluid flows in the direction of the

HSET forward movement. Meantime, the fluid flows along the entrance of the tunnel in the direction of the TC.

When the HC exits the tunnel, a counterclockwise rotating vortex appears on the nose tip of the HC, which part of the fluid in this vortex flows away from the flow field at the exit of the tunnel with the direction of rotation, while another part flows into the exit of the tunnel and towards the entrance of the tunnel with the direction of rotation. It is also seen that two vortices with opposite rotation directions appear at the left and right front of the tunnel exit, as displayed in Figure 8.

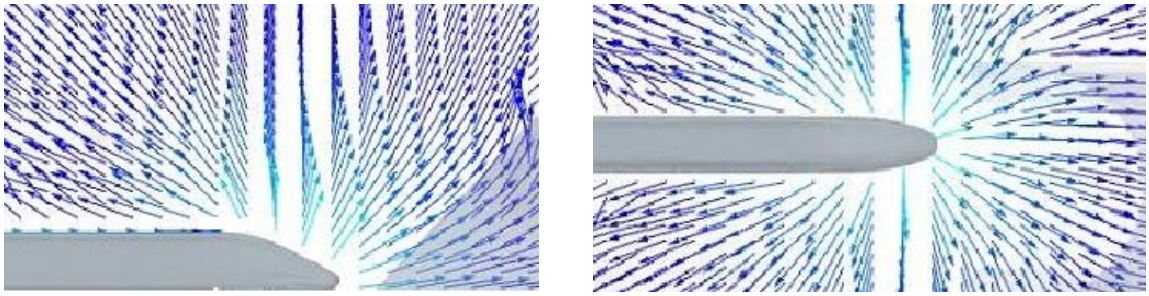

(a) Front view (b) Top view

Figure 4. Distribution of external velocity field when the HC runs in non-tunnel areas

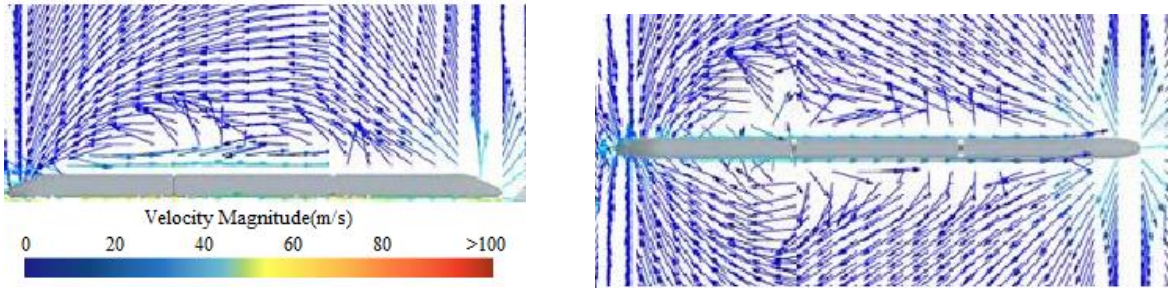

(a) Front view (b) Top view

Figure 5. Distribution of external velocity field when HSET runs in non-tunnel areas

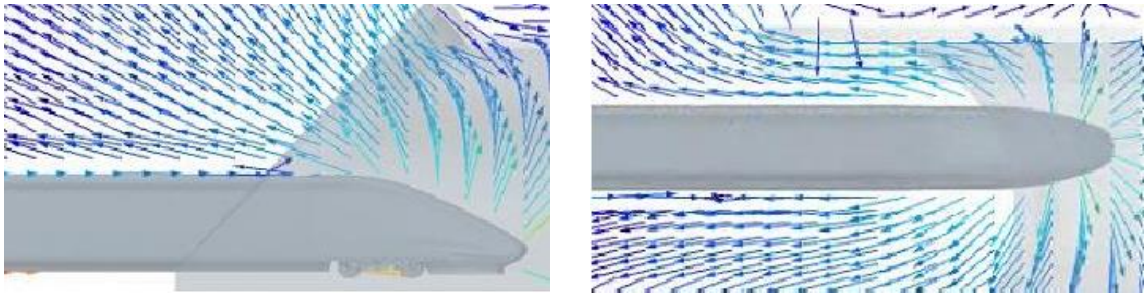

(a) Front view (b) Top view

Figure 6. Distribution of external velocity field when the HC enters the tunnel

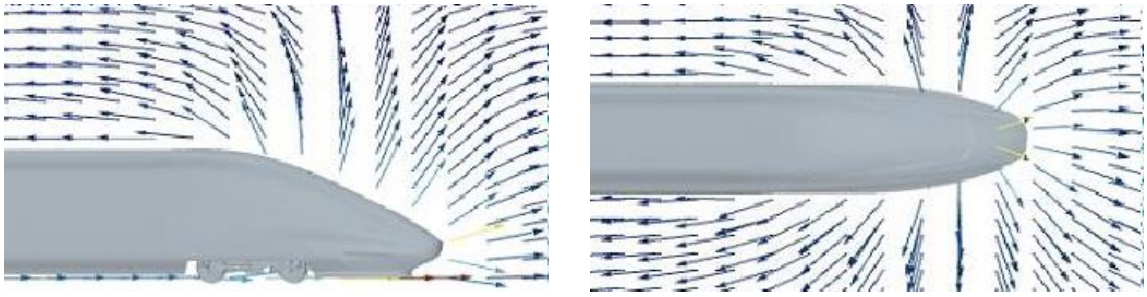

(a) Front view (b) Top view

Figure 7. Distribution of external velocity field when HSET runs inside the tunnel

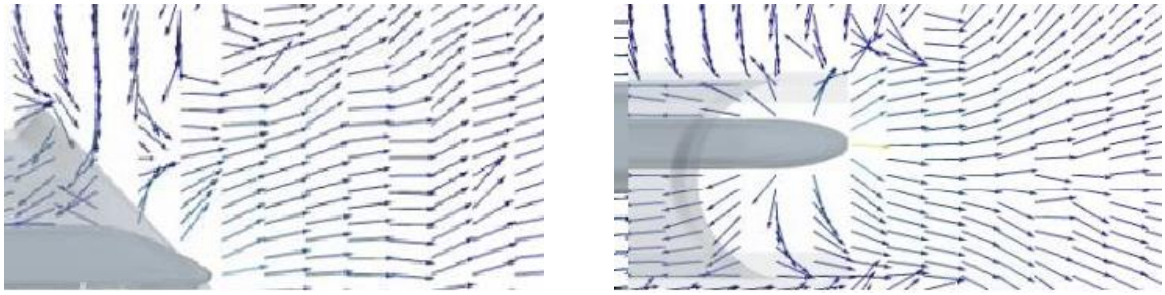

(a) Front view (b) Top view

Figure 8. Distribution of external velocity field when the HC exits the tunnel

4.2 Influence of speed on the aerodynamic drag of the HSET

As shown in Figure 8, when the speed of HSET is equal to 200 km/h and 300 km/h, the HC enters the tunnel in 1.8 seconds and 1.3 seconds, and exits the tunnel in 8.5 seconds and in 6.0 seconds, respectively. When the HC enters the tunnel, the aerodynamic drag increases significantly, and the greater the HSET speed, the greater the amplitude of the drag experienced by the HC. It is evident that the maximum aerodynamic drag occurs within the tunnel area. When the HSET fully enters the tunnel, the drag of the HC decreases, but when the HSET completely exits the tunnel, the difference in aerodynamic of the HC is small at different speeds.

Meantime, the curve of the aerodynamic drag of the MC over time is shown in Figure 9, where the MC enters the tunnel in 2.5 seconds and 1.6 seconds, and exits the tunnel in 9.2 seconds and in 6.4 seconds, when the speed of HSET is equal to 200 km/h and 300 km/h, respectively. It is obvious that the trend of the drag of the MC is the same, and the amplitude of the drag increases with the increase of HSET speed. When the HSET runs, the MC is subjected to aerodynamic drag. When the MC enters the tunnel from the non-tunnel area, the drag experienced by the MC first increases to its peak and then remains stable. When the MC enters the open track through the tunnel and is subjected to crosswind, the drag further increases. When the HSET completely exits the tunnel, the aerodynamic drag amplitude of the MC remains basically unchanged.

The curve of the aerodynamic drag of the TC is displayed in Figure 10, when the speed of HSET is equal to 200 km/h and 300 km/h, the TC enters the tunnel in8.7 seconds and 2seconds, and exits the tunnel in 9.7 seconds and in 6.8 seconds, respectively. It is seen that the trend of the drag over time is the same at different speeds, and the amplitude of the drag increases with the increase of HSET speed. When the HSET runs, the TC is subjected to aerodynamic drag. Once the HSET enters the tunnel from the non-tunnel area, the aerodynamic drag on the TC first increases to its peak and then remains stable. When the TC enters the non-tunnel area through the tunnel, the aerodynamic drag of the TC begins to decrease and gradually stabilizes. At different speeds, the drag experienced by the TC is in the negative direction, and the amplitude of the aerodynamic drag increases with the increase of the speed.

The typical aerodynamic drag distribution at different speeds and positions (P1, P2, P3 and P4) is given in Table 1, where the maximum aerodynamic drag of the HSET occurs inside the tunnel, and the aerodynamic drag of the HSET is the highest (44.52kN).

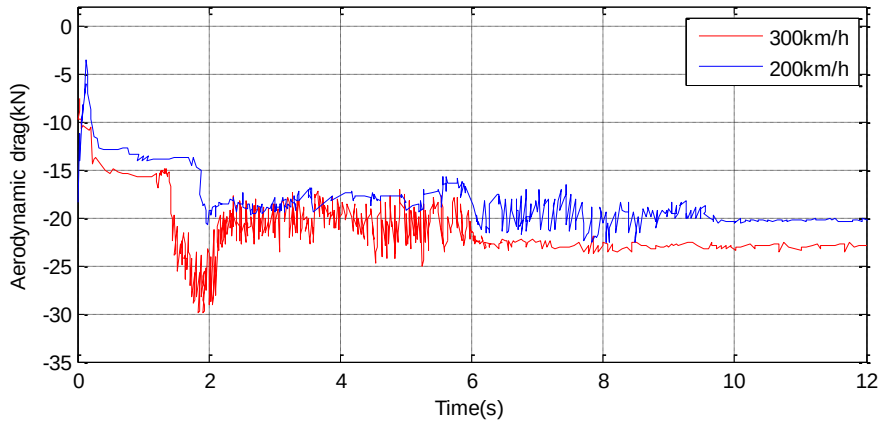

Figure 8. Aerodynamic drag of the HC at different speeds

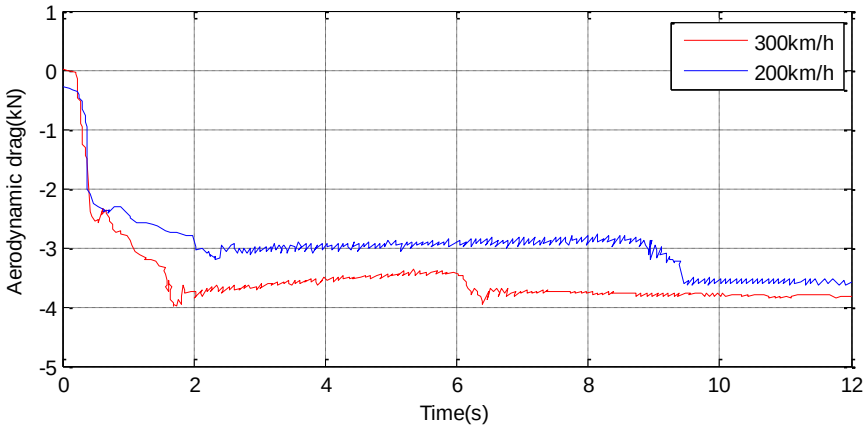

Figure 9. Aerodynamic drag of the MC at different speeds

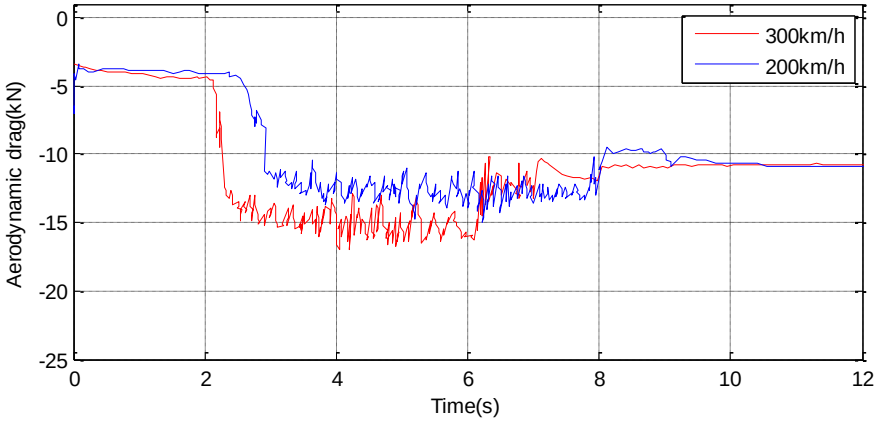

Figure 10. Aerodynamic drag of the TC at different speeds

Table 1 The maximum aerodynamic drag at different positions (unit: kN)

Position	P1(200, 300km/h)	P2(200,300km/h)	P3(200,300km/h)	P4(200,300km/h)
HC	14.41, 16.24	5.52, 6.43	11.52, 28.60	10.45, 9.29
MC	3.21, 3.72	2.92, 3.35	2.95, 3.51	2.83, 3.67
TC	13.43, 14.47	4.72, 4.97	11.81,12.41	10.12, 11.47
HSET	32.05, 13,83	13.16, 14.75	26.28, 44.52	23.4, 24.43

V. Conclusions

When the HSET runs in non-tunnel areas, a clear train wind is formed around the HSET. Along the direction from the HC to the TC, the thickness of the train wind gradually increases, and vortex separation phenomenon also appears.

When the HSET runs at a high speed inside the tunnel, the boundary between the curved body and the windshield near the nose of the HC is located, and the fluid flows in the direction of the HSET forward movement, meanwhile the fluid flows along the entrance of the tunnel in the direction of the TC.

When the HSET runs the tunnel, the expansion wave generated by the TC entering the tunnel reaches the HC, the aerodynamic drag of the HC reaches its maximum value of 29.85 kN, and the aerodynamic drag of the HSET also reaches its maximum value of 44.52 kN when the speed of the HSET is equal to 300 km/h.

Acknowledgments

The work is supported by National Natural Science Foundation of China (No. 51475386). The authors thank above organizations for support, and thank anonymous reviewers for their valuable comments.

References

[1]. Muld T W, Efraimsson G, Dan S H (2012) Flow structures around a high-speed train extracted using proper orthogonal decomposition and dynamic mode decomposition. Computers and Fluids, 57 (10): 87-97.

[2]. Chu CR, Chen S Y, Wang C Y, et al (2014) Numerical simulation of two trains intersecting in a tunnel. Tunnelling and Underground Space Technology, 42: 161-174.

[3]. Kikuchi K, Suzuki M (2015) Study of aerodynamic coefficients used to estimate critical wind speed for vehicle overturning. Journal of Wind Engineering and Industrial Aerodynamics, 147: 1-17.

[4]. Soper D, Baker C, Sterling M (2015) An experimental investigation to assess the influence of container loading configuration on the effects of a crosswind on a container freight train. Journal of Wind Engineering and Industrial Aerodynamics, 145: 304-317.

[5]. Bell J R, Burton D, Thompson M C, et al (2015) Moving model analysis of the slipstream and wake of a high-speed train. Journal of Wind Engineering and Industrial Aerodynamics, 136: 127-137.

[6]. Li Q L, SunYQ, Ouyang M H, et al (2024) Flow and sound fields of scaled high-speed trains with different coach numbers running in long tunnel. Railway Engineering Science, 32(3):401-420.

[7]. Xie P, Peng Y, Wang T et al (2020) Aural comfort prediction method for high-speed trains under complex tunnel environments. Transportation Research Part D: Transport and Environment, 81:102284.

[8]. Ferrari S, Hu Y, Martinuzzi RJ, et al (2017) Visualizing vortex clusters in the wake of a high-speed train. IEEE International Conference on Systems, Man, and Cybernetics,7: 683–688.

[9]. Wu J F, Li X Z, Cai C S, et al (2022) The influence of the leading-edge angle of subgrade on the aerodynamic loads of a high-speed train in a wind tunnel. RailwayEngineering Science, 30(2):221-241.

[10]. Niu J Q, Wang Y M, Liu F, et al (2021) Numerical study on comparison of detailed flow field and aerodynamic performance of bogies of stationary train and moving train. Vehicle System Dynamic, 59(12):1844–1866.